Available online at www.sciencedirect.com

SciVerse ScienceDirect

Ceramics International 38 (2012) 5871–5878

CERAMICS INTERNATIONAL

www.elsevier.com/locate/ceramint

Bulk synthesis of ZnO nanoparticles by the one-step electromagnetic levitational gas condensation method

M. Vaghayenegar, A. Kermanpur *, M.H. Abbasi

Department of Materials Engineering, Isfahan University of Technology, Isfahan 84156-83111, Iran

Received 25 March 2012; accepted 11 April 2012
Available online 19 April 2012

Abstract

The ZnO nanoparticles were synthesized by the one-step electromagnetic levitational gas condensation method with a relatively high production rate. In this method, the vapors ascending from a high temperature levitated Zn droplet were condensed and oxidized by He–0.2Ar and O_2 gas mixtures, respectively, under both atmospheric and reduced pressures. Effects of carrier gas type and temperature, oxygen content, and reactor pressure on the size, size distribution and morphology of the particles were investigated. The particles were characterized by X-ray diffraction, scanning electron microscopy and transmission electron microscopy methods. The production rate of the crystalline ZnO nanoparticles was estimated as high as 300 g h^{-1}. The results showed that decreasing the gas temperature and reactor pressure resulted in a smaller particle size and a higher fraction of rod-like nanoparticles.

Keywords: A. Powders: gas phase reaction; D. ZnO; Levitation melting; Nanoparticles

1. Introduction

Zinc oxide (ZnO) is a well-known n-type semiconductor with a wide band gap and high excitation binding energy. ZnO has been used in many diverse applications such as antibacterial [1], nanoprism probe for nanooptical applications [2], MEMs [3], solar cells [4], ultraviolet light emitting diodes [5], thin-film transistors [6], pizoelectric transducers [7], varistors [8], and gas sensors [9,10]. Recently, a great attention has been paid upon the properties of ZnO to adopt it for different applications. The optical and electronic properties of semiconductors can be further tuned by varying the size of the particles in the nanometric range.

Nanoparticles of ZnO attract an increasing interest due to their possible use in a range of new nanodevices. ZnO nanoparticles have more than fourteen different morphologies, among which considerable attention has been focused on tetrapod-like and rod-like ones because of their promising applications in optics [11]. For example, it is shown that despite the good intrinsic electronic properties of ZnO, simple nanocrystalline ZnO electrodes were found to have very poor photovoltaic properties with solar energy conversion efficiency of lower than 1% [12]. Recently reported nanostructured ZnO electrode showed slightly improved values of 1.5–3.9%. Such low photovoltaic properties of ZnO are mainly related with the unstable surface chemistry of ZnO to acidic dye molecule. In this regard, it is shown that the rod-like array ZnO electrode showed stable photovoltaic properties compared with nano-particulate electrode despite the small adsorption of dye molecules [12]. The well-crystallized surface of the nanorods should reduce significantly the formation of Zn^{2+}–dye aggregates. The rod-like array electrode is also favorable for electrolyte diffusion since the diffusion channel is highly spacious and hardly blocked by Zn^{2+}–dye aggregates within the electrode, while the complicated nano-pore channels in nano-particulate electrode can be easily blocked. In addition, ZnO whiskers were presented as a useful reinforcement material due to its high-temperature strength and excellent chemical stability [13].

ZnO nanoparticles have been so far synthesized with different methods like pulsed laser ablation [11], magnetron RF Plasma [14], thermal evaporation [15], spray pyrolysis [16], diffusion flame [17], sol–gel [18], hydrothermal [19], sonochemical [20], microemulsions [21] and many combined, assisted and novel routes. Critical issues in the fabrication of compound nanoparticles mainly include their purity, size and

* Corresponding author. Tel.: +98 311 3915738; fax: +98 311 3912752.
E-mail address: ahmad_k@cc.iut.ac.ir (A. Kermanpur).

0272-8842/$36.00
http://dx.doi.org/10.1016/j.ceramint.2012.04.038

size distribution, and production rate. In the present work, ZnO nanoparticles have been synthesized with a novel approach named as electromagnetic levitational gas condensation (ELGC) method. This method is capable of direct synthesis of pure and crystalline nanoparticles with a relatively high production rate. In this method, the sample is levitated in the magnetic field of a special design of the induction coil carrying an alternative current. The specimen is then heated, melted and finally evaporated. The metal vapors are then condensed by the cold inert gas stream flowing upward in the reactor and the particles are collected in a filtering system. Bigot and Champion [22,23] reported the first attempts on using the electromagnetic levitation melting for synthesis of metal nanoparticles. They used liquid nitrogen/argon for condensing the metal vapors. Rhee et al. [24] have synthesized nanoparticles of some metals and oxides using the ELGC method. Recently, Kermanpur et al. have synthesized nanoparticles of Fe [25], Al [26] and Zn [27] with this method. Due to the difficulties in the levitation melting of alloys, no extensive works have been reported so far on the use of this technology for the synthesis of different nanomaterials. In the present work, pure ZnO nanoparticles were directly synthesized with the ELGC method using different gas carriers of Ar and He–0.2Ar with O_2 as the oxidizing gas under atmospheric and reduced pressures. Effects of process parameters on the size and size distribution of ZnO nanoparticles were discussed. The formation mechanism of the nanorods is discussed based on the physical models elsewhere [28].

2. Materials and methods

The schematics of the ELGC experimental set-up are shown in Fig. 1. The system is equipped with a high frequency induction power supply with working power and frequency of 45 kW and 450 kHz, respectively. Bulk Zn sample with the purity of 99.91% was levitated in the magnetic field of a suitable induction coil. This induction coil is usually consisted of two parts; the lower part is the main windings which produces a levitation force (lifting part) and the upper part is the controlling turns which are necessary to insure levitation stability (stabilizing part). The latter part is connected in series with the former, but their winding directions are just opposite to each other (as shown in Fig. 1). The electromagnetic potential well (null point) is located at the gap between these two parts of a complete coil. Once the current is introduced to the coil, eddy currents are induced in the body. Interaction of the eddy currents with the imposed magnetic field gives rise to a Lorentz force that can support the conducting sample against gravity. In addition, the eddy currents can heat, melt and finally vaporize the body. Besides supporting the sample, the Lorentz force causes a flow in the molten droplet. In the present work, design of the suitable coil was determined by finite element simulation of electromagnetic forces exerted to the levitated specimen [29]. The sample was melted and started evaporation rapidly. The Zn vapors were then condensed by an inert carrier gas (Ar or He–0.2Ar with the purity of 99.999%) and the condensed particles were eventually collected in a bubble filter. In order to synthesize ZnO nanoparticles, Zn vapors were oxidized by introducing pure O_2 (99.999%) gas into the reactor at the onset of Zn evaporation. Effects of O_2 content in the gas stream on crystallinity and morphology of the nanoparticles were investigated.

Morphology, size and crystallinity of ZnO particles were characterized by transmission electron microscopy (TEM Philips CM120), scanning electron microscopy (SEM Philips XL30), X-ray diffraction (XRD Philips X'Pert with Cu-Kα anode) and the image analysis software of Image Tools.

3. Results and discussion

3.1. Effect of oxygen content and carrier gas type on particle size

Two types of carrier gas (Ar and He–0.2Ar) were used to condense the particles. Fig. 2 shows XRD patterns of particles synthesized at different gas molar ratios of O_2/Ar under atmospheric pressure. Fig. 2a corresponds to XRD pattern of

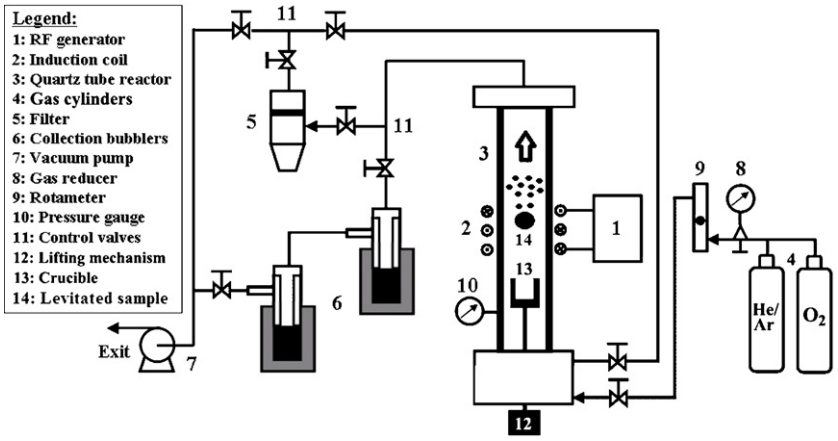

Fig. 1. Schematics of the electromagnetic levitational gas condensation system. As shown, the sample (14) is levitated inside the induction coil (2). At the same time, the metal vapors ascending from the levitated sample are condensed by the He/Ar cooling gas flowing upward inside the tube reactor (3). The synthesized particles are moved up (as shown by an arrow in the reactor) and eventually collected in a filter (5) or collection bubbles (6).

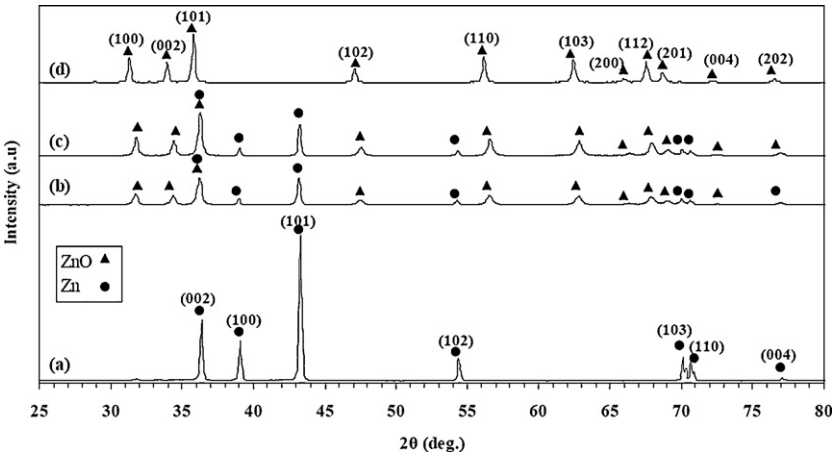

Fig. 2. XRD patterns of the particles synthesized under atmospheric pressure at different O_2/Ar gas molar ratios of: (a) 0, (b) 0.06, (c) 0.10 and (d) 0.12. Ar is the carrier and cooling gas, while O_2 is the oxidizing agent. It can be seen that introducing O_2 gas into the reactor resulted in a decrease in the intensity of Zn peaks and an increase in the intensity of ZnO peaks. The molar ratio of O_2/Ar = 0.12 resulted in a fully ZnO particles.

the particles synthesized using oxygen-free Ar, in which only peaks corresponding to pure crystalline Zn can be seen in agreement with the data from JCPDS card No. 04-0831. The XRD patterns of the particles with introducing O_2 gas into the reactor show that a decrease in the intensity of Zn peaks and an increase in the intensity of ZnO peaks is occurred by increasing the molar ratio of O_2/Ar (Fig. 2b–d). The XRD pattern of the particles synthesized with the molar ratio of O_2/Ar = 0.12 shows that all Zn characteristic peaks were vanished (see Fig. 2d). This pattern is in agreement with the JCPDS card No. 36-1451 which corresponds to the hexagonal wurtzite structure of ZnO. The sample temperature and molar production rate under this condition were estimated 1400 °C and 0.04 mol min^{-1}, respectively. Fig. 3 shows SEM micrographs of ZnO particles synthesized under atmospheric pressure with the O_2/Ar molar ratio of 0.12. As it can be seen, the particles are mostly in the form of rods and a smaller amount of tetrapods. The mean length and the mean width of ZnO particles were measured as 290.6 and 132.4 nm, respectively. It should be noted that due to the instability in the droplet levitation, it was not possible to increase the molar ratio of O_2/Ar more than about 0.12. This may be due to the formation of a thick oxide layer over the droplet and hence becoming nonconductor.

Fig. 4 shows XRD patterns of particles synthesized at different gas molar ratios of O_2/He–0.2Ar under atmospheric pressure. The XRD patterns of the particles with introducing O_2 gas into the reactor show that increasing the molar ratio of O_2/He–0.2Ar resulted in a decrease in the intensity of Zn peaks and an increase in the intensity of ZnO peaks (Fig. 4b–d). The XRD pattern of the particles synthesized with the molar ratio of O_2/He–0.2Ar = 0.18 shows that all Zn characteristic peaks were vanished (see Fig. 4d). The sample temperature and molar production rate under this condition were estimated 1235 °C and 0.028 mol min^{-1}, respectively. Fig. 5a and b shows TEM micrographs of ZnO particles synthesized under atmospheric pressure with the O_2/He–0.2Ar molar ratio of 0.18. As it can be seen, the particles are mostly in the form of rods and a smaller amount of tetrapods. The mean length and the mean width of ZnO particles were measured as 94.7 and 54.7 nm, respectively. It is seen that the particle size is decreased by using the carrier gas of He–0.2Ar compared to that of Ar. The reason for the difference in particle size is due to the lower atomic weight of He atoms compared to that of Ar atoms (4.0 g mol^{-1} vs. 40.0 g mol^{-1}, respectively). As nucleation and subsequently condensation of the particles in the ELGC method is performed by collision of the metal vapors with inert gas atoms, the hot metal vapors can gain more energy from the heavier inert gas atoms by collision and consequently results in a higher

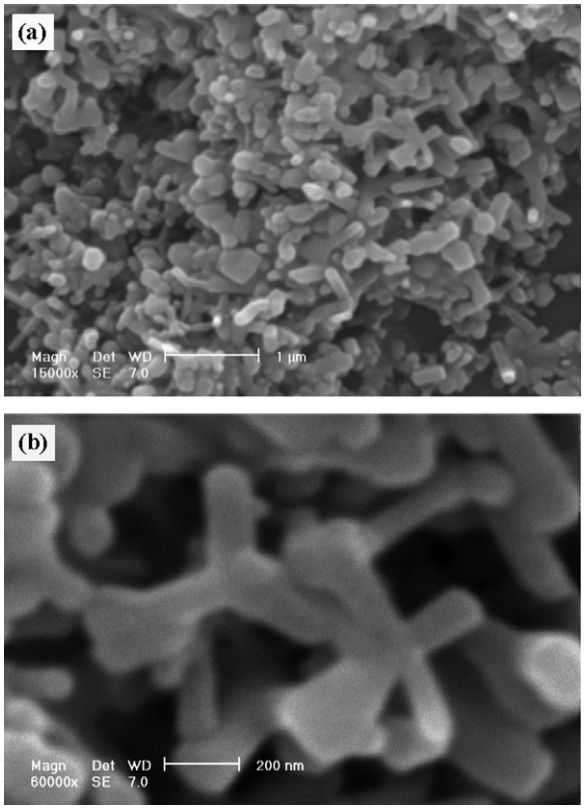

Fig. 3. SEM micrographs of ZnO particles synthesized under atmospheric pressure at O_2/Ar = 0.12 in two magnifications. It can be seen that the particles are mostly in the form of rods and tetrapods. The mean length and the mean width of ZnO particles were measured as 290.6 and 132.4 nm, respectively.

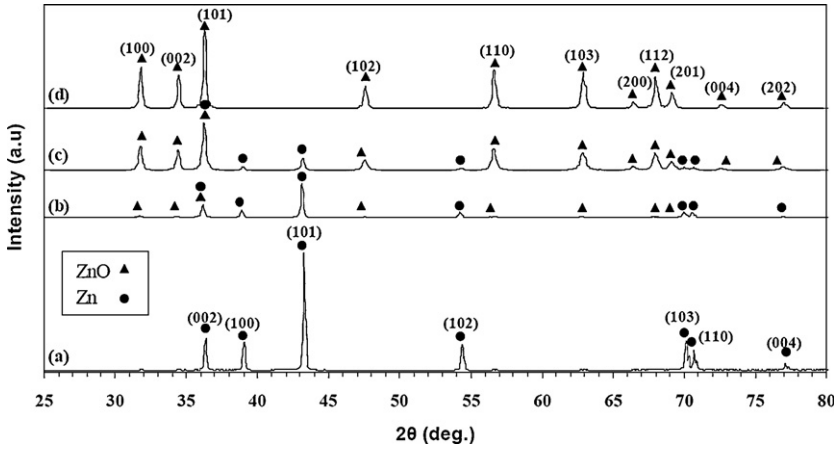

Fig. 4. XRD patterns of the particles synthesized under atmospheric pressure at different O_2/He–0.2Ar gas molar ratios of: (a) 0, (b) 0.13, (c) 0.15 and (d) 0.18. He–0.2Ar is the carrier and cooling gas, while O_2 is the oxidizing agent. It can be seen that introducing O_2 gas into the reactor resulted in a decrease in the intensity of Zn peaks and an increase in the intensity of ZnO peaks. The molar ratio of O_2/He–0.2Ar = 0.18 resulted in fully ZnO particles.

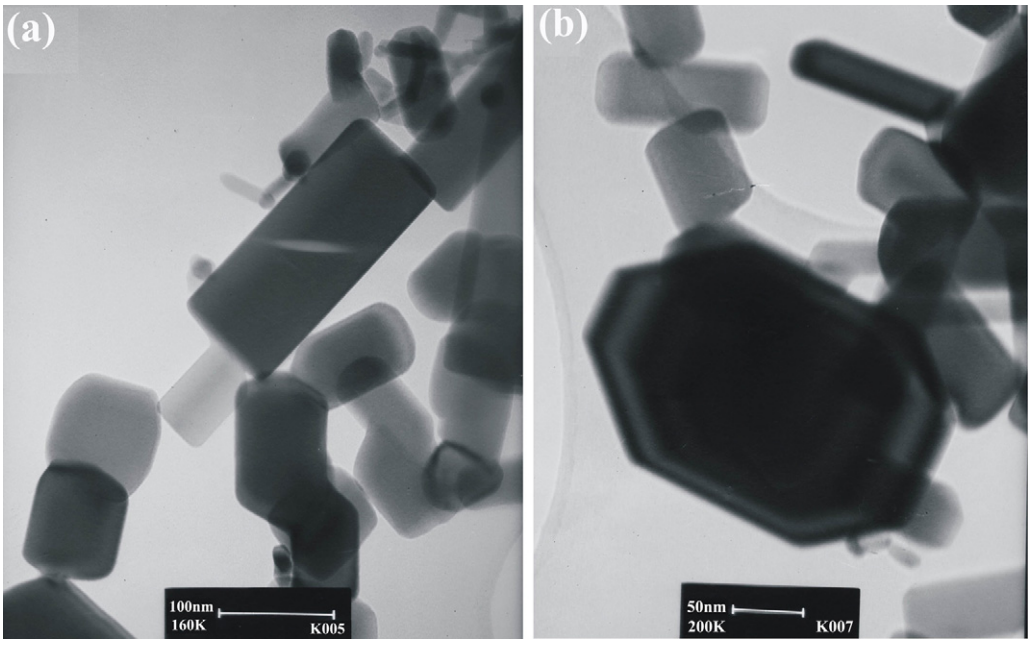

Fig. 5. TEM micrographs of ZnO particles synthesized under atmospheric pressure at O_2/He–0.2Ar = 0.18 in two magnifications. It can be seen that the particles are mostly in the form of rods and tetrapods. The mean length and the mean width of ZnO particles were measured as 94.7 and 54.7 nm, respectively.

undercooling and growth rate for metal clusters. Moreover, the lower thermal conductivity of the Ar (0.0177 $Wm^{-1} K^{-1}$) compared to that of He–0.2Ar (0.1513 $Wm^{-1} K^{-1}$) makes the entire gas mixture to cool slower. Therefore, the particles condensed by the Ar atoms should have larger size compared to those formed by the He–0.2Ar gas. This effect has already been shown by Kermanpur et al. for the synthesis of Zn NPs [27].

3.2. Effect of carrier gas temperature on particle size

In order to investigate the effect of gas temperature on size and morphology of the particles, O_2 and He–0.2Ar (with the molar ratio of 0.18) were passed through a sufficient long copper coil immersed in liquid N_2 before introducing to the reactor. The decrease in gas temperature was measured to be about 75 K. The sample temperature and molar production rate under this condition were estimated 1200 °C and 0.025 mol min^{-1}, respectively. TEM micrographs of ZnO particles synthesized under atmospheric pressure with the N_2-cooled gas with the O_2/He–0.2Ar molar ratio of 0.18 are shown in Fig. 6. The particles are again in the form of rods and tetrapods, but their mean length and mean width of ZnO particles are reduced to 79.7 and 35.4 nm, respectively. It is seen that decreasing temperature resulted in a smaller particle size due to making restriction in particle growth. Fig. 6c shows XRD pattern of the particles synthesized using the cooled gas mixture (with the O_2 to He–0.2Ar molar ratio of 0.18). This pattern is in agreement with characteristics peaks of the hexagonal wurtzite structure of ZnO.

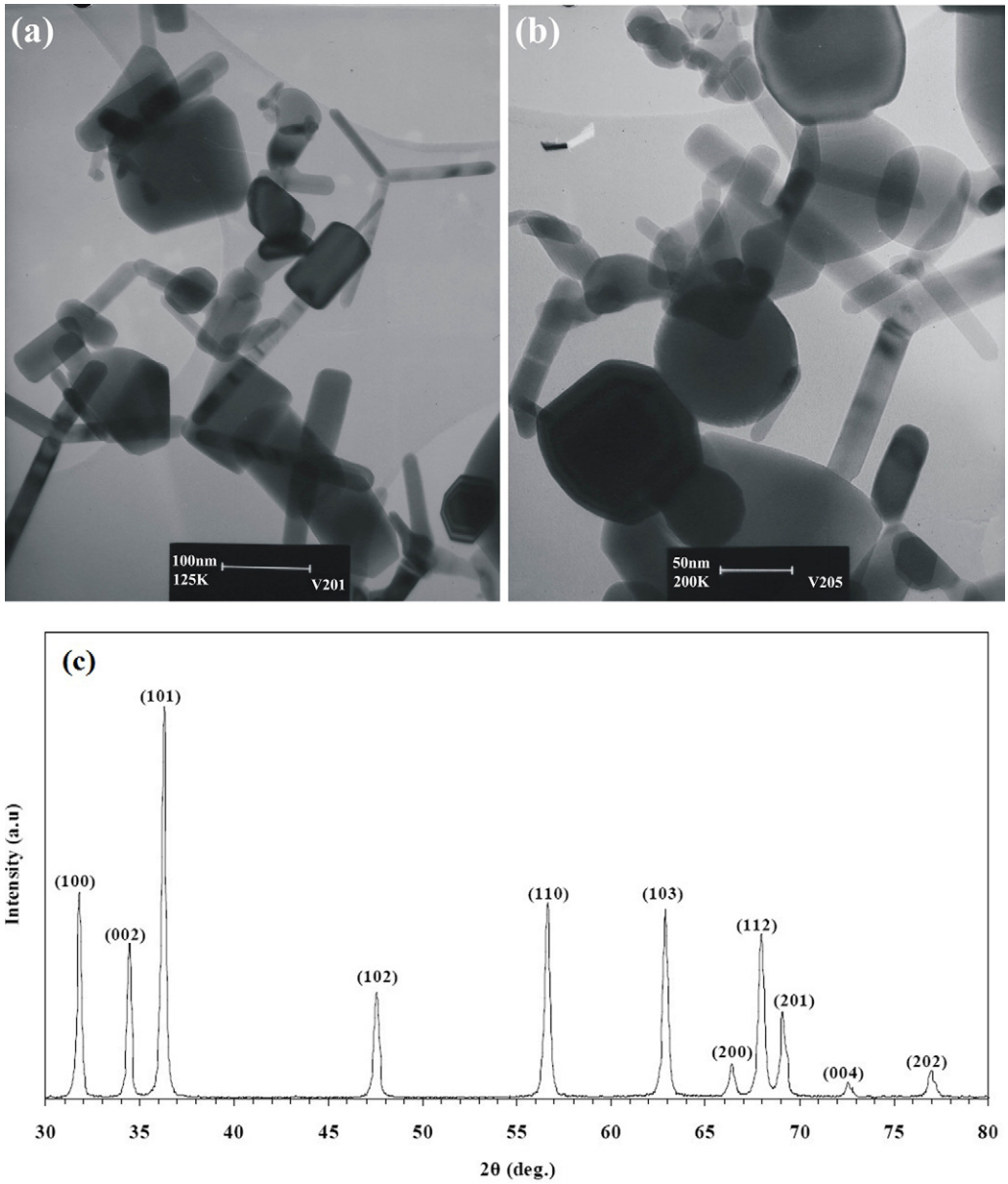

Fig. 6. (a and b) TEM micrographs and (c) XRD pattern of ZnO particles synthesized under atmospheric pressure at O_2/He–0.2Ar = 0.18 using a cooled carrier gas. It can be seen that the particles are mostly in the form of rods and tetrapods. Due to the use of cooled carrier gas, the mean length and the mean width of ZnO particles are reduced to 79.7 and 35.4 nm, respectively.

3.3. Effect of reactor pressure on particle size

The reactor pressure is another important process parameter in the ELGC method. The molar production rate at 330 mmHg was higher than the atmospheric condition (0.048 mol min^{-1} vs. 0.028 mol min^{-1}, respectively). TEM micrographs of ZnO particles synthesized under the reduced pressure of 330 mmHg, shown in Fig. 7, reveal again particles with the rods and tetrapods morphologies. The mean length and width of ZnO particles under the reduced pressure were 83.3 and 26.6 nm, respectively. Fig. 7c shows XRD patterns of the particles synthesized at different gas molar ratios of O_2/He–0.2Ar under the pressure of 330 mmHg. A similar trend can be seen. The XRD pattern of the particles synthesized with the molar ratio of O_2/He–0.2Ar = 0.21 shows that all Zn characteristic peaks were vanished and the product is pure ZnO.

The present results showed that decreasing the reactor pressure led to a smaller particle size. This can be explained in terms of the molecular mean free path. In kinetic theory, the *mean free path* of a particle, such as a molecule, is the average distance the particle travels between collisions with other moving particles. If the velocities of the identical particles have a Maxwell distribution, the following relationship applies for determining the mean free path, λ [30]:

$$\lambda = \frac{RT}{\sqrt{2}\pi d^2 N_A P} \quad (1)$$

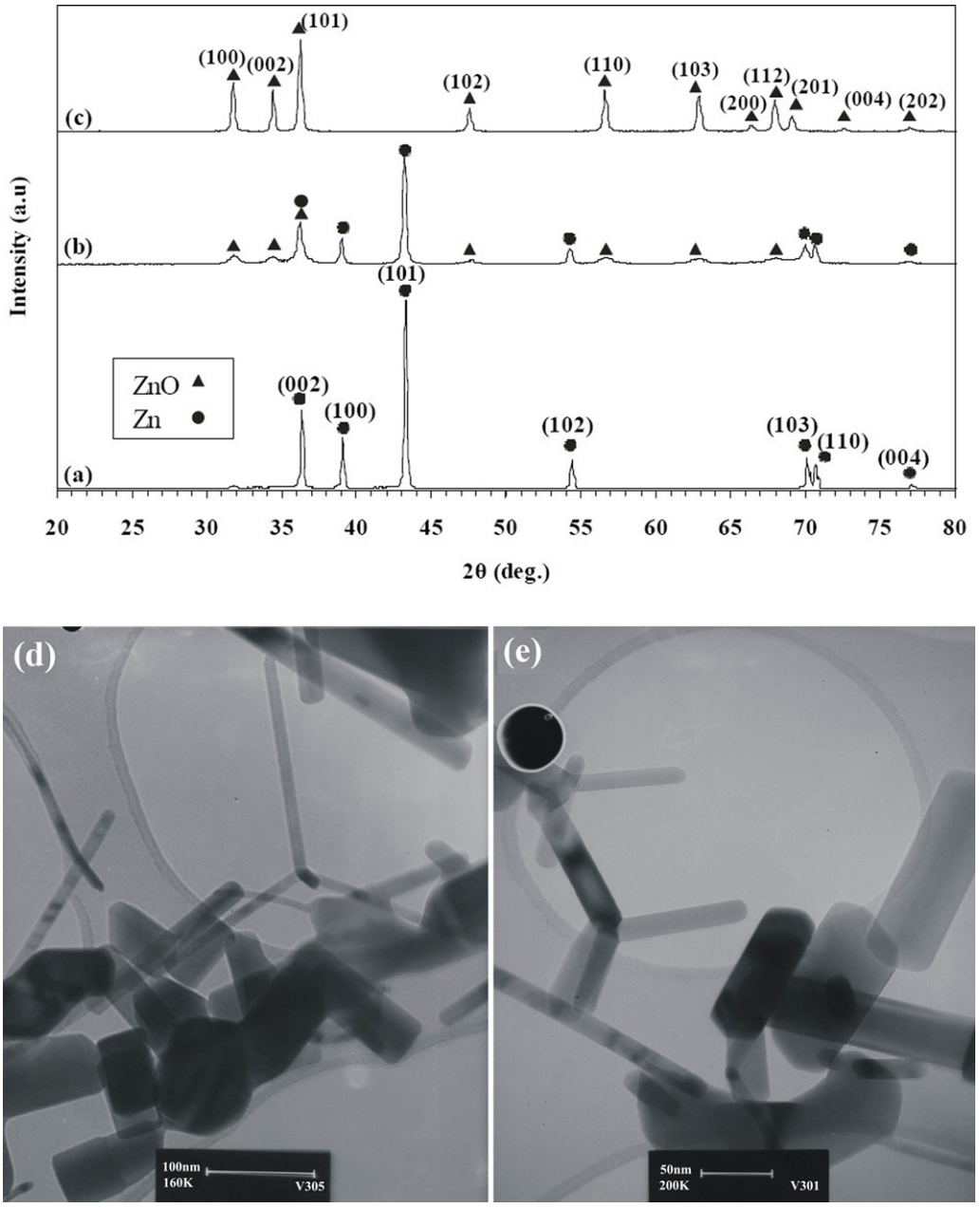

Fig. 7. XRD patterns of ZnO particles synthesized at the pressure of 330 mm Hg with different O_2/He–0.2Ar gas molar ratios of: (a) 0, (b) 0.13 and (c) 0.21. (d–e) TEM micrographs of ZnO particles synthesized at O_2/He–0.2Ar = 0.21 under the pressure of 330 mm Hg. It is revealed that the particles have mostly rod and tetrapod morphologies. Due to the synthesis of particles under the reduced pressure of 330 mm Hg, the mean length and width of ZnO particles are reduced to 83.3 and 26.6 nm, respectively.

where T is temperature, P is pressure, d is the diameter of the gas particles, R is the gas constant and N_A is the Avogadro constant. Assuming the gas temperature to be constant, it is clearly seen that by decreasing gas pressure in the system, the mean free path is increased. As a higher mean free path of the atoms causes a lower contingency of particle collision during synthesis, a smaller particle size is achieved under reduced pressure. It should be pointed out that as temperature of the levitated droplet, and hence gas temperature, in the ELGC process is mainly related to the coil design, the affecting parameter here is the reactor pressure.

3.4. Effect of process parameters on morphology of particles

According to the specific morphology of the particles, the concept of aspect ratio (i.e. length/width) was used to compare size distribution of the particles synthesized under different conditions. These distributions are illustrated in Fig. 8. It is clearly noticeable that there is a higher percentage of particles with length/width = 1 under atmospheric condition. However, the results show that decreasing the gas temperature and/or reactor pressure, resulted in a more volume fraction of the

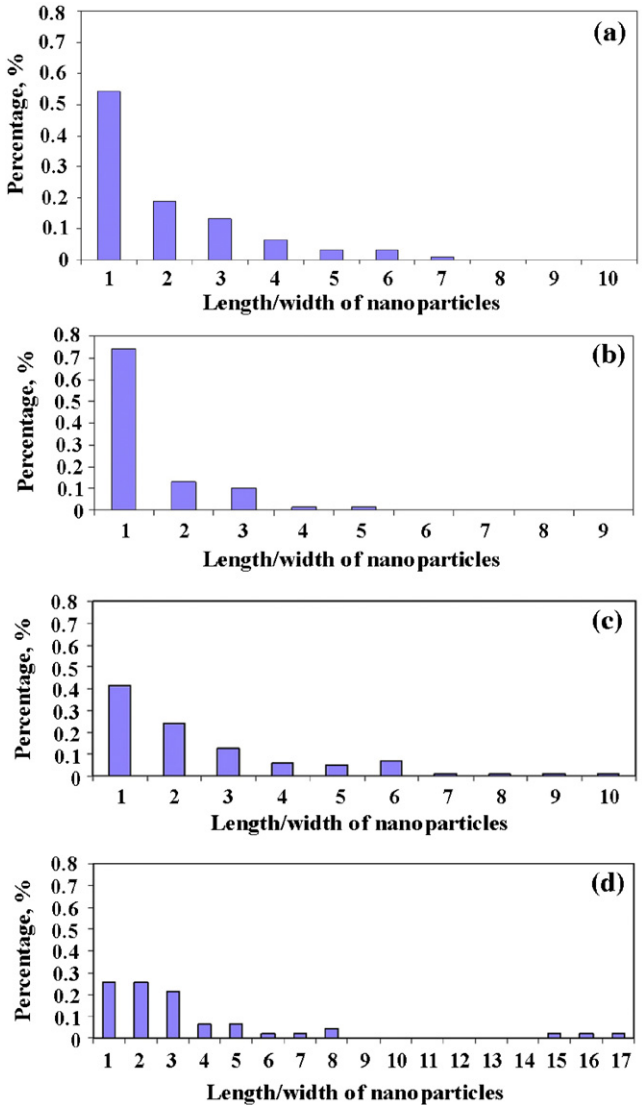

Fig. 8. Size distribution of ZnO particles in different sets of aspect ratios under: (a) atmospheric pressure of Ar, (b) atmospheric pressure of He–0.2Ar, (c) atmospheric pressure of cooled He–0.2Ar and (d) reduced pressure (330 mm Hg) of He–0.2Ar. A higher percentage of particles have the aspect ratio of length/width = 1 under atmospheric condition. The percentage of this aspect ratio is decreased with decreasing of pressure and temperature.

nanorods with the higher length/width ratios. Therefore, it is possible to change the particle morphology through process parameters.

3.5. The production rate of the ELGC method

Scale-up production is of great interest for nanoparticle synthesis. High energy ball milling, already a commercial high volume process, has been instrumental in generating nanoparticles for the preparation of magnetic, structural, and catalytic materials [31]. However, the process produces polydispersed amorphous powder, which requires subsequent partial recrystallization before the powder is consolidated into nanostructured materials. For sol–gel processing, the development of continuous processing techniques based on present knowledge of batch processing has yet to be addressed for economical scale-up production of nanoparticles. Other related sol–gel issues concern the cost of precursors and the recycling of solvent [31]. The gas phase methods of nanoparticles synthesis have low production rates. In research laboratories, this rate is typically in the 100 mg h^{-1} range. A number of different aerosol methods have been developed for increasing the production rate of nanoparticles, but each of them has its merits and drawbacks [31]. In the present work, the production rate for the synthesis of ZnO nanoparticles by the ELGC method was estimated about 300 g h^{-1}. This rate is much higher than that of most of the gas phase methods. The results presented above clearly show that the ELGC method can be used as a bulk process for the formation of ZnO nanoparticles in the commercial scale. The particle morphology can be controlled via process parameters.

4. Conclusions

In the present study, the feasibility of direct synthesis of ZnO nanorods with the production rate of about 300 g h^{-1} was illustrated by the electromagnetic levitational gas condensation method. The results showed that reducing gas temperature and reactor pressure both led to the formation of smaller ZnO nanoparticles and a higher fraction of nanorods. The optimum O_2/He–0.2Ar molar gas ratio to synthesize fully oxidized particles was found as 0.18 and 0.21 for both atmospheric and reduced pressures with the mean length/width of about 80/35 and 83/27 nm, respectively.

References

[1] Y. Liu, L. He, A. Mustapha, H. Li, Z. Hu, M. Lin, Antibacterial activities of zinc oxide nanoparticles against *Escherichia coli* O157:H7, Journal of Applied Microbiology 107 (2009) 1193–1201.
[2] T. Kim, D.S. Kim, B.Y. Lee, Z.H. Kim, S. Hong, Nanoprism, Probe for nano-optical applications, Advanced Materials 21 (2009) 1238–1242.
[3] R. Singh, M. Kumar, S. Chandra, Growth and characterization of high resistivity *c*-axis oriented ZnO films on different substrates by RF magnetron sputtering for MEMS applications, Journal of Materials Science 42 (2007) 4675–4683.
[4] M. Krunks, A. Katerski, T. Dedova, I. Oja Acik, A. Mere, Nanostructured solar cell based on spray pyrolysis deposited ZnO nanorod array, Solar Energy Materials and Solar Cells 92 (2008) 1016–1019.
[5] W.S. Han, Y.Y. Kim, B.H. Kong, H.K. Cho, Ultraviolet light emitting diode with n-ZnO:Ga/i-ZnO/p-GaN:Mg heterojunction, Thin Solid Films 517 (2009) 5106–5109.
[6] D.J. Yun, S.W. Rhee, Deposition of Al-doped ZnO thin-films with radio frequency magnetron sputtering for a source/drain electrode for pentacene thin-film transistor, Thin Solid Films 517 (2009) 4644–4649.
[7] D. Zaouk, Y. Zaatar, R. Asmar, J. Jabbour, Piezoelectric zinc oxide by electrostatic spray pyrolysis, Microelectronics Journal 37 (2006) 1276–1279.
[8] Q. Wang, Y. Qin, G.J. Xu, L. Chen, Y. Li, L. Duan, Z.X. Li, Y.L. Li, P. Cui, Low-voltage ZnO varistor fabricated by the solution-coating method, Ceramics International 14 (2008) 1697–1701.
[9] P. Sŭlcova, M. Trojan, New green pigments; ZnO–CoO, Dyes Pigments 40 (1999) 83–86.
[10] A.B. Kashyout, H.M.A. Soliman, H. Shokry Hassan, A.M. Abousehly, Fabrication of ZnO and ZnO:Sb nanoparticles for gas sensor applications, Journal of Nanomaterials (2010) 8 (Article ID 341841).

[11] C. He, T. Sasaki, Y. Shimizu, N. Koshizaki, Synthesis of ZnO nanoparticles by pulsed laser ablation in aqueous media and their self-assembly towards spindle-like ZnO aggregates, Applied Surface Science 254 (2008) 2196–2202.
[12] K.S. Kim, Y.S. Kang, J.H. Lee, Y.J. Shin, N.G. Park, K.S. Ryu, S.H. Chang, Photovoltaic properties of nano-particulate and nanorod array ZnO electrodes for dye-sensitized solar cell, Bulletin of the Korean Chemical Society 27 (2006) 295–298.
[13] J.Q. Hu, X.L. Ma, Z.Y. Xie, N.B. Wong, C.S. Lee, S.T. Lee, Characterization of zinc oxide crystal whiskers grown by thermal evaporation, Chemical Physics Letters 344 (2001) 97–100.
[14] S.-F. Wang, T.-Y. Tseng, Y.-R. Wang, C.-Y. Wang, H.-C. Lu, Effect of ZnO seed layers on the solution chemical growth of ZnO nanorod arrays, Ceramics International 35 (2009) 1255–1260.
[15] B.H. Kong, H.K. Cho, Formation of vertically aligned ZnO nanorods on ZnO templates with the preferred orientation through thermal evaporation, Journal of Crystal Growth 289 (2006) 370–375.
[16] M. Breedon, M.B. Rahmani, S.H. Keshmiri, W. Wlodarski, K. Kalantar-zadeh, Aqueous synthesis of interconnected ZnO nanowires using spray pyrolysis deposited seed layers, Materials Letters 64 (2010) 291.
[17] R. Maric, M. Oljaca, B. Vukasinovic, A.T. Hunt, Synthesis of oxide nanopowders in nanospray diffusion flames, Materials and Manufacturing Processes 19 (2004) 1143–1156.
[18] M. Vafaee, M. Sasani Ghamsari, Preparation and characterization of ZnO nanoparticles by a novel sol–gel route, Materials Letters 61 (2007) 3265–3268.
[19] Y.-. Wang, J. Sun, X.Y. Fan, X. Yu, A CTAB-assisted hydrothermal and solvothermal synthesis of ZnO nanopowders, Ceramics International 37 (2011) 3431–3436.
[20] S.H. Jung, S.H. Jeong, Selective-area growth of ZnO nanorod arrays via a sonochemical route, Materials Letters 62 (2008) 3673–3675.
[21] H. Lu, X. Yu, Z. Zeng, D. Chen, K. Bao, L. Zhang, H. Wang, H. Xu, R. Zhang, DC-field-induced synthesis of ZnO nanowhiskers in water-in-oil microemulsions, Ceramics International 37 (2011) 287–292.
[22] J. Bigot, Preparation and properties of nanocrystalline powders obtained by cryogenic melting, Annales de Chimie France. 18 (1993) 369–378.
[23] Y. Champion, J. Bigot, Synthesis and structural analysis of aluminum nanocrystalline powders, Nanostructured Materials 10 (1998) 1097–1110.
[24] Y.R. Uhm, B.S. Han, M.K. Lee, S.J. Hong, C.K. Rhee, Synthesis and characterization of nanoparticles of ZnO by levitational gas condensation, Materials Science and Engineering A 449–451 (2007) 813–816.
[25] A. Kermanpur, B. Nekooei Rizi, M. Vaghayenegar, H. Ghasemi Yazdabadi, Bulk synthesis of monodisperse Fe nanoparticles by electromagnetic levitational gas condensation method, Materials Letters 63 (2009) 575–577.
[26] A. Kermanpur, M.R. Dadfar, B. Nekooei Rizi, M. Eshraghi, Synthesis of aluminum nanoparticles by electromagnetic levitational gas condensation method, Journal of Nanoscience and Nanotechnology 10 (2010) 6251–6255.
[27] M. Vaghayenegar, A. Kermanpur, M.H. Abbasi, H. Ghasemi Yazdabadi, Effects of process parameters on synthesis of Zn ultrafine/nanoparticles by electromagnetic levitational gas condensation, Advanced Powder Technology 21 (2010) 556–563.
[28] M. Vaghayenegar, A. Kermanpur, M.H. Abbasi, Formation mechanism of ZnO nanorods produced by the electromagnetic levitational gas condensation method, Scientia Iranica 18 (2011) 1647–1651.
[29] A. Kermanpur, M. Jafari, M. Vaghayenegar, Electromagnetic-thermal coupled simulation of levitation melting of metals, Journal of Materials Processing Technology 211 (2011) 222–229.
[30] S. Chapman, T.G. Cowling, The Mathematical Theory of Non-Uniform Gases, 3rd. ed., Cambridge University Press, 1990,, p. 88.
[31] R.W. Siegel, E. Hu, M.C. Roco, Nanostructure Science and Technology—A Worldwide Study, National Science and Technology Council, September, 1999.